Acta Crystallographica Section F
Structural Biology and Crystallization Communications
ISSN 1744-3091

The structure of an orthorhombic crystal form of a 'forced reduced' thiol peroxidase reveals lattice formation aided by the presence of the affinity tag

Katherine S. H. Beckham,[a] Olwyn Byron,[b] Andrew J. Roe[a]* and Mads Gabrielsen[a]*

[a]Institute of Infection, Immunity and Inflammation, College of Medical, Veterinary and Life Sciences, University of Glasgow, Sir Graeme Davies Building, Glasgow G12 8QQ, Scotland, and [b]School of Life Sciences, College of Medical, Veterinary and Life Sciences, University of Glasgow, Sir Graeme Davies Building, Glasgow G12 8QQ, Scotland

Correspondence e-mail: Andrew.Roe@glasgow.ac.uk, mgabr@chem.gla.uk

Received 9 February 2012
Accepted 16 March 2012

PDB Reference: C61S mutant of Tpx, 4af2.

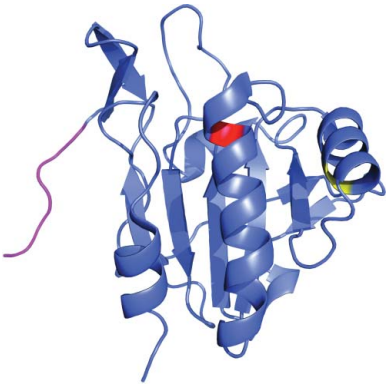

Thiol peroxidase (Tpx) is an atypical 2-Cys peroxiredoxin, which has been suggested to be important for cell survival and virulence in Gram-negative pathogens. The structure of a catalytically inactive version of this protein in an orthorhombic crystal form has been determined by molecular replacement. Structural alignments revealed that Tpx is conserved. Analysis of the crystal packing shows that the linker region of the affinity tag is important for formation of the crystal lattice.

1. Introduction

Thiol peroxidase (Tpx) is an atypical 2-Cys peroxiredoxin found in both Gram-negative and Gram-positive bacteria (Cha *et al.*, 1995). Tpx is a redox-active protein that reduces alkyl peroxides and hydrogen peroxide through the catalytic recycling of a disulfide bond between cysteines 61 and 95. This cycle results in the production of water, with reduced Tpx being regenerated through interaction with thioredoxin (Baker & Poole, 2003). Tpx makes a major contribution to redox homeostasis in the bacterial cell. For example, *Escherichia coli* Tpx deletion mutants displayed reduced survival after exposure to peroxide (Cha *et al.*, 1995). Furthermore, this protein has been shown to be important for the survival of human pathogens such as *Salmonella typhimurium*, in which the ability to withstand the oxidative burst in the phagosome is essential (Horst *et al.*, 2010). Tpx has also been implicated in the virulence of Gram-negative pathogens as it has been shown to be one of the target proteins of the salicylidene acylhydrazides (Wang *et al.*, 2011). These so-called 'anti-virulence' compounds inhibit the bacterial type 3 secretion system, which is used by pathogens to modulate host-cell pathways and facilitate disease (Baron, 2010).

Here, we describe the crystallization and structure analysis of the catalytically inactive mutant TpxC61S from *E. coli*, which represents a 'forced reduced' structure as described by Hall *et al.* (2009). The crystals diffracted to 1.97 Å resolution and exhibited an orthorhombic form. A brief comparison of this structure with a number of structures of Tpx present in the Protein Data Bank, including a trigonal crystal form of the same mutant from *E. coli* (Hall *et al.*, 2009), is presented. Analysis of the crystal packing of the two TpxC61S structures reveals the importance of parts of the affinity tag in forming crystal contacts in the orthorhombic space group.

2. Materials and methods

2.1. Cloning, expression and purification

The C61S mutant of Tpx was obtained by site-directed mutagenesis utilizing a QuikChange site-directed mutagenesis kit (Stratagene) with the primer pair ecTpx5/3 (CGTACTGATGCGGCCGAAACACCGGTATC and GATACCGGTGTTTCGGCCGCATCAGTACG); the construct was confirmed by DNA sequencing. The amplified product was cloned into the TOPO pET-151 (Invitrogen) expression vector, which encodes an N-terminal affinity tag consisting of a hexahistidine sequence motif with a TEV cleavage site and a linker region consisting of 25 residues. The resulting construct was transformed into *E. coli* BL21 DE3 (λD3) cells and grown in 1 l LB

medium containing ampicillin (100 µg ml^{-1}). The protein was purified using immobilized metal-affinity chromatography protocols as described elsewhere (Gabrielsen *et al.*, 2010) and dialysed against 20 m*M* Tris pH 7.5, 50 m*M* NaCl.

2.2. Crystallization

Purified protein with affinity tag at approximately 8 mg ml^{-1} was screened by sitting-drop vapour diffusion using several commercial crystallization screens with 1 µl drops consisting of a 1:1 ratio of protein and reservoir solutions. The crystal trays were incubated at 293 K. Crystals appeared in the JCSG+ Suite (Molecular Dimensions Ltd) after two weeks against a reservoir consisting of 0.2 *M* $MgCl_2$, 0.1 *M* Tris pH 7, 10% polyethylene glycol 8000. The crystal was cryoprotected by a short soak in paraffin oil (Riboldi-Tunnicliffe & Hilgenfeld, 1999) before being flash-cooled in liquid nitrogen.

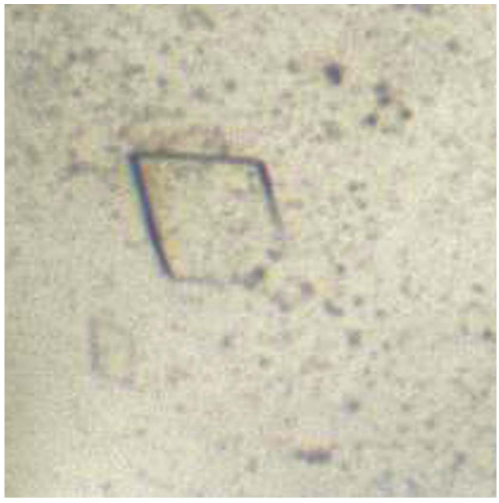

(*a*)

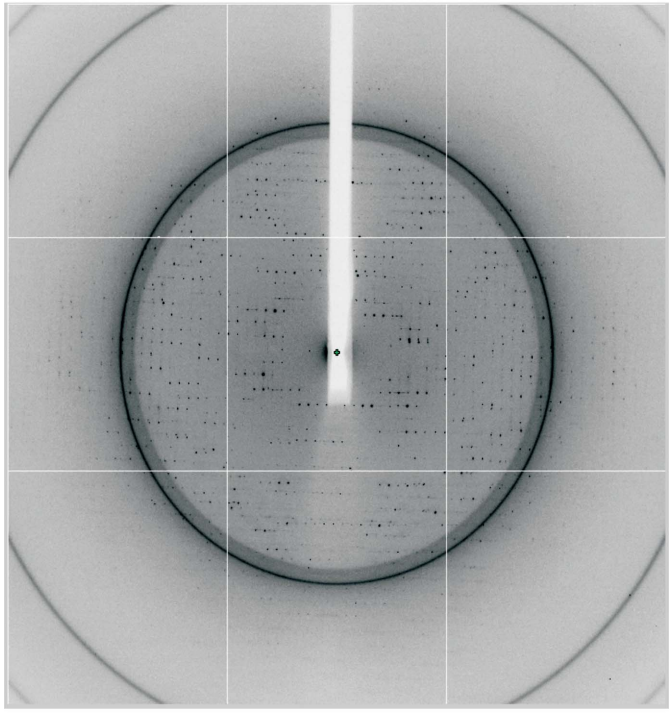

(*b*)

Figure 1
E. coli TpxC61S crystals and diffraction. (*a*) The orthrombic crystals have dimensions of 0.1 × 0.1 × 0.3 mm. (*b*) The crystals diffracted to 1.97 Å resolution (at the detector edge) and belonged to space group $C222_1$.

Table 1
Data-collection and refinement statistics.

Values in parentheses are for the highest resolution shell.

PDB code	4a2f
Space group	$C222_1$
Unit-cell parameters (Å)	a = 49.37, b = 71.75, c = 121.93
Resolution (Å)	40.67–1.97 (2.08–1.97)
Observed reflections	96980
Unique reflections	15679
Multiplicity	6.2 (6.6)
Completeness (%)	90.2 (100)
R_{meas}† (%)	14.2 (67.5)
$R_{p.i.m.}$‡ (%)	5.7 (26.0)
$\langle I/\sigma(I)\rangle$	7.5 (2.8)
Wilson B factor (Å^2)	19.9
Matthews coefficient (Å^3 Da^{-1})	3.09
Solvent content (%)	60.16
Water O atoms	170
R_{work} (%)	22.93
R_{free} (%)	28.28
R.m.s.d. for bond lengths (Å)/angles (°)	0.009/1.17
Average isotropic thermal parameters (Å^2)	
Main chain	35.34
Side chain	40.95
Water O atoms	37.53
Ramachandran outliers	0
MolProbity clash score	6.57 [94th percentile]

† $R_{meas} = \sum_{hkl}\{N(hkl)/[N(hkl)-1]\}^{1/2}\sum_i |I_i(hkl) - \langle I(hkl)\rangle|/\sum_{hkl}\sum_i I_i(hkl)$.
‡ $R_{p.i.m.} = \sum_{hkl}\{1/[N(hkl)-1]\}^{1/2}\sum_i |I_i(hkl) - \langle I(hkl)\rangle|/\sum_{hkl}\sum_i I_i(hkl)$.

2.3. X-ray data measurements, structure solution and refinement

Diffraction data were collected using an ADSC Q315 CCD detector on Diamond Light Source beamline I04 at a wavelength of 0.9763 Å. Data were processed using *MOSFLM* (Leslie, 1992) and scaled and merged using *SCALA* (Evans, 2006) from the *CCP*4 suite (Winn *et al.*, 2011). The structure of TpxC61S was determined using *Phaser*; the existing TpxC61S structure from *E. coli* (PDB entry 3hvv; Hall *et al.*, 2009) was used as a search model for molecular replacement. The structure was refined using *REFMAC*5 (Murshudov *et al.*, 2011) and *BUSTER* (Bricogne *et al.*, 2011). The model was manipulated as required and waters were added using *Coot* (Emsley *et al.*, 2010). The model was validated using *Coot* and *MolProbity* (Chen *et al.*, 2010). *PISA* was used to analyze protein interfaces and crystal contacts (Krissinel & Henrick, 2007) and structural superpositions were performed using the SUPER command in *PyMOL* (Schrödinger; http://www.pymol.org). Figures were produced using *ALINE* (Bond & Schüttelkopf, 2009) and *PyMOL*.

The structure and data were deposited in the Protein Data Bank (Velankar *et al.*, 2012; accession code 4af2).

3. Results and discussion

3.1. Crystallization, data collection and structure determination

The crystals of the C61S mutant of Tpx from *E. coli* were orthorhombic, with dimensions of approximately 0.1 × 0.1 × 0.03 mm (Fig. 1*a*), and belonged to space group $C222_1$, with unit-cell parameters a = 49.37, b = 71.75, c = 121.93 Å. Data were collected to a resolution of 1.97 Å (Fig. 1*b*), and the relevant data-collection statistics are presented in Table 1. The asymmetric unit comprised one subunit with a Matthews coefficient of 3.09 Å^3 Da^{-1}, indicating a solvent content of 60%. The data processed well, with overall R_{meas} and $R_{p.i.m.}$ values of 14.2% and 5.7%, respectively.

The molecular-replacement solution was refined to final R_{work} and R_{free} values of 22.9% and 28.3%, respectively. There are no outliers in the Ramachandran plot and the structure is in the 94th percentile of *MolProbity* clash scores (Chen *et al.*, 2010). All relevant structure-refinement statistics are listed in Table 1.

3.2. Overall structure of TpxC61S

TpxC61S exhibits a thioredoxin-like fold with a seven-stranded β-sheet flanked by four α-helices, with an additional two N-terminal β-strands that are typical for Tpx but are not found in other peroxiredoxin structures (Fig. 2). Owing to the mutation of the active cysteine residue to a serine, the structure is locked in the reduced confirmation. This conformation has an elongated α1 helix, which makes Cys61 available for interactions with H_2O_2 or alkyl peroxides; however, the presence of the mutation to serine prevents these interactions. Following oxidation of Cys61, helix α1 becomes unravelled to form an intramolecular disulfide bond with residue Cys95 (Hall *et al.*, 2009; Gabrielsen *et al.*, 2012). The conformational change observed in response to redox state is shown in Fig. 3(*b*).

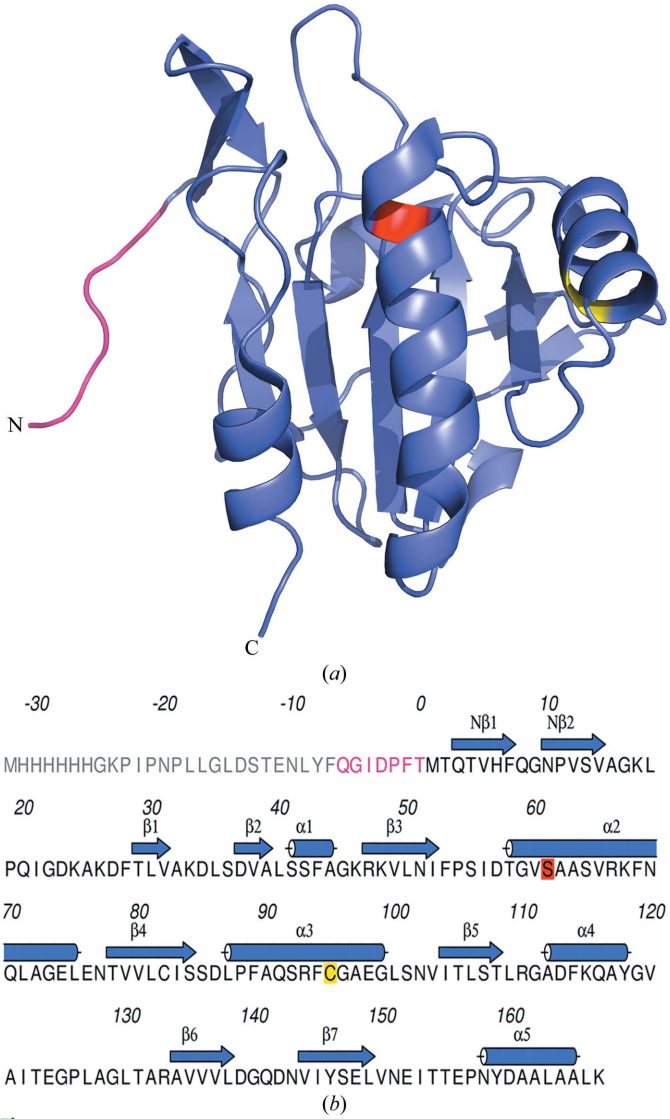

Figure 2
The structure of orthorhombic TpxC61S compared with existing structures. (*a*) The overall structure of TpxC61S is shown with Ser61 (red) and Cys95 (yellow) highlighted. The N- and C-termini of the protein have been labelled, along with the secondary-structure elements. (*b*) The sequence of the purified and crystallized protein with secondary-structure elements indicated above and the catalytic residues highlighted. The affinity tag is shown in grey, with the part of the tag that can be observed in electron density shown in pink.

Table 2
Superposition of orthorhombic TpxC61S with reduced wild-type and 'forced reduced' mutated Tpx structures.

The oxidized Tpx from *E. coli* (PDB entry 3hvs) has been added for completeness.

Species	PDB code
Escherichia coli	3hvv
Yersinia pseudotuberculosis	2xpd
Y. pseudotuberculosis	2yjh
Mycobacterium tuberculosis	1y25
Streptococcus pneumoniae	1psq
E. coli	3hvs

Tpx forms a homodimer in solution (Baker & Poole, 2003; Gabrielsen *et al.*, 2012). In this crystal structure the dimer is formed by a crystallographic symmetry-related molecule. The structure of TpxC61S superposes well onto other crystal structures of reduced Tpx (Table 2). In particular, this mutant superposes with the wild-type reduced protein from *Yersinia pseudotuberculosis* (Gabrielsen *et al.*, 2012) with a root-mean-square deviation (r.m.s.d.) of 0.376 Å, indicating a high degree of similarity (Fig. 3*a*). This confirms the assumption made by Hall *et al.* (2009) that TpxC61S represents a 'forced reduced' structure. When compared with the oxidized *E. coli* structure (PDB entry 3hvs; Hall *et al.*, 2009), TpxC61S superposes with an r.m.s.d. of 0.711 Å. This reflects the local conformational change between the oxidized and the reduced structure mediated by the formation of a disulfide bond between Cys61 and Cys95 (Fig. 3*b*).

3.3. Analysis of the crystal lattice

The orthorhombic form of TpxC61S superposes well onto the existing trigonal TpxC61S structure (PDB entry 3hvv; Hall *et al.*, 2009) with an r.m.s.d. of 0.207 Å, showing that despite the different space groups ($C222_1$ and $P3_121$, respectively) the structure remains essentially the same (Fig. 2*b*). However, when investigating the crystal packing, a noticeable difference between the two crystal forms became apparent. The unit cell of the trigonal form of TpxC61S is much more densly packed, with a solvent content of 42%. In contrast, orthorhombic TpxC61S has a solvent content of 60%. This explains the difference in the crystal contacts formed between the monomeric asymmetric unit and its environment. Whilst the trigonal crystal form has ten neighbouring TpxC61S molecules within 5.0 Å, the orthorhombic form has only six.

Despite the more spacious packing of the protein in $C222_1$, the crystals diffract similarly and are robust. When analyzing the crystal lattice, the linker region of the affinity-tag construct, which is accounted for in the electron density in orthorhombic TpxC61S, is involved in several crystal contacts and thus stabilizes the crystal through facilitating lattice formation (Fig. 4*a*).

Analysis of the crystal packing in the orthorhombic crystal lattice using the *Protein Interfaces, Surfaces and Assemblies* (*PISA*) server (Krissinel & Henrick, 2007) revealed that 17% of the total surface area of 8349 Å^2 was buried. The largest buried area occurs at the dimerization interface of the protein, which accounts for about half of the buried surface area. The rest of the crystal contacts are formed between the linker region of the affinity tag of one molecule and a neighbouring molecule, as shown in Fig. 4(*b*), with a smaller second crystal contact with another subunit. The area of contact conferred by the linker region is stabilized by two hydrogen bonds between the tag

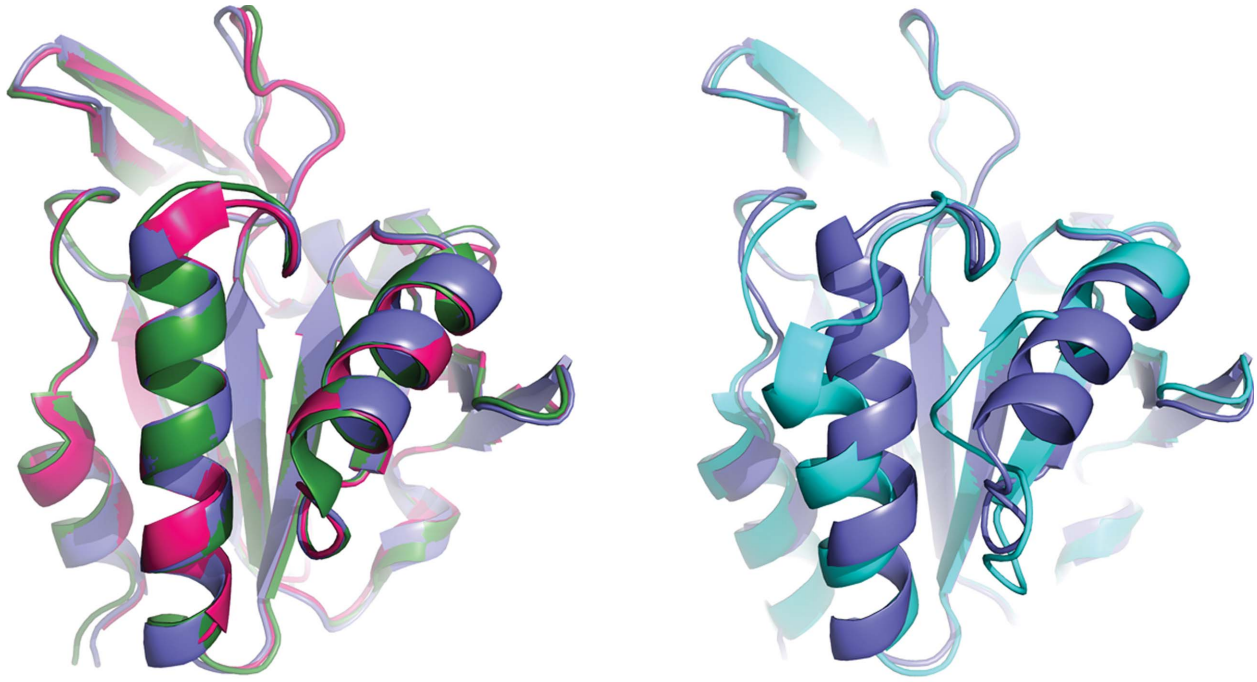

(*a*) (*b*)

Figure 3
Comparison of TpxC61S with existing Tpx structures. (*a*) Superposition of orthorhombic TpxC61S (slate) with trigonal TpxC61S (PDB entry 3hvv; Hall *et al.*, 2009; pink; *E. coli*) and reduced wild-type Tpx (PDB entry 2xpd; Gabrielsen *et al.*, 2010; green; *Y. pseudotuberculosis*) illustrates the high level of similarity between this structure, the existing TpxC61S structure from *E. coli* and that of reduced wild-type Tpx. (*b*) Orthorhombic TpxC61S (slate) superimposes less well with oxidized wild-type Tpx (cyan; PDB entry 3hvs; Hall *et al.*, 2009) owing to the confirmational change caused by the differing redox states.

(Ile−4 and Phe−1) and a symmetry-related molecule (Lys′33) (Fig. 4*b*). In comparison, the buried surface area between trigonal TpxC61S and symmetry-related neighbours makes up around 10% of the total surface area. However, each subunit makes direct crystal contacts with eight symmetry-related molecules. This highlights the importance of the tag in stabilizing TpxC61S in the orthorhombic form.

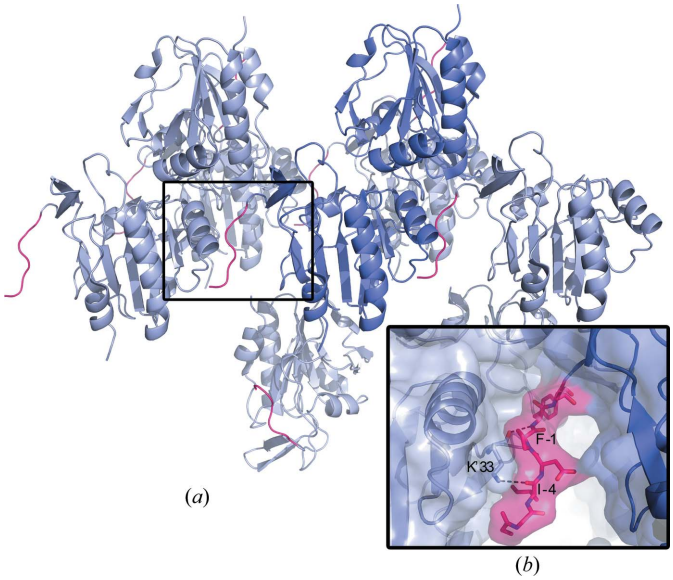

(*a*) (*b*)

Figure 4
Crystal packing of TpxC61S. (*a*) The crystal lattice formed in the orthorhombic crystal form of TpxC61S highlights the importance of the linker region of the affinity tag (pink) in forming crystal contacts. The biological dimer formed by crystallographic symmetry is shown in slate, with other molecules in the crystal lattice shown in light blue. (*b*) A detailed view of the crystal contacts between the linker region and a symmetry-related molecule highlighted in the black box shown in (*a*). The residues involved in hydrogen-bond formation have been labelled, namely Lys′33 N^{ζ} to Ile−4 N (3.2 Å) and Lys′33 O to Phe−1 O (3.1 Å). Hydrogen bonds are shown as dashed lines.

4. Conclusions

We have reported the structure of an orthorhombic crystal form of TpxC61S from *E. coli* at 1.97 Å resolution. The overall structure is well conserved amongst known homologues and this mutant form is a good representation of the reduced form of Tpx. The crystal lattice is held in place by the linker region of the affinity tag of one subunit attaching to a neighbouring unit, threading throughout the lattice.

We thank the Diamond Light Source for access to beamline I04 (proposal No. MX1229). This work was supported by a grant from the Biotechnology and Biological Sciences Research Council to MG and AJR (BB/G011389/1), a Medical Research Scotland Grant (223 ORG) to AJR and a Wellcome Trust Studentship for KSHB. We acknowledge Karen McLuskey for discussions and thorough reading of the manuscript.

References

Baker, L. M. & Poole, L. B. (2003). *J. Biol. Chem.* **278**, 9203–9211.
Baron, C. (2010). *Curr. Opin. Microbiol.* **13**, 100–105.
Bond, C. S. & Schüttelkopf, A. W. (2009). *Acta Cryst.* D**65**, 510–512.
Bricogne, G., Blanc, E., Brandl, M., Flensburg, C., Keller, P., Paciorek, W., Roversi, P., Sharff, A., Smart, O. S., Vonrhein, C. & Womack, T. O. (2011). *BUSTER* v.2.8.0. Cambridge: Global Phasing Ltd.
Cha, M.-K., Kim, H.-K. & Kim, I.-H. (1995). *J. Biol. Chem.* **270**, 28635–28641.

Chen, V. B., Arendall, W. B., Headd, J. J., Keedy, D. A., Immormino, R. M., Kapral, G. J., Murray, L. W., Richardson, J. S. & Richardson, D. C. (2010). *Acta Cryst.* D**66**, 12–21.
Emsley, P., Lohkamp, B., Scott, W. G. & Cowtan, K. (2010). *Acta Cryst.* D**66**, 486–501.
Evans, P. (2006). *Acta Cryst.* D**62**, 72–82.
Gabrielsen, M., Beckham, K. S. H., Feher, V. A., Zetterström, C. Z., Wang, D., Müller, S., Elofsson, M., Amaro, R. E., Byron, O. & Roe, A. J. (2012). *PLoS One*, **7**, e32217.
Gabrielsen, M., Zetterström, C. E., Wang, D., Beckham, K. S. H., Elofsson, M., Isaacs, N. W. & Roe, A. J. (2010). *Acta Cryst.* F**66**, 1606–1609.
Hall, A., Sankaran, B., Poole, L. B. & Karplus, P. A. (2009). *J. Mol. Biol.* **393**, 867–881.
Horst, S. A., Jaeger, T., Denkel, L. A., Rouf, S. F., Rhen, M. & Bange, F. C. (2010). *J. Bacteriol.* **192**, 2929–2932.
Krissinel, E. & Henrick, K. (2007). *J. Mol. Biol.* **372**, 774–797.
Leslie, A. G. W. (1992). *Jnt CCP4/ESF–EACBM Newsl. Protein Crystallogr.* **26**.
Murshudov, G. N., Skubák, P., Lebedev, A. A., Pannu, N. S., Steiner, R. A., Nicholls, R. A., Winn, M. D., Long, F. & Vagin, A. A. (2011). *Acta Cryst.* D**67**, 355–367.
Riboldi-Tunnicliffe, A. & Hilgenfeld, R. (1999). *J. Appl. Cryst.* **32**, 1003–1005.
Velankar, S. *et al.* (2012). *Nucleic Acids Res.* **40**, D445–D452.
Wang, D. *et al.* (2011). *J. Biol. Chem.* **286**, 29922–29931.
Winn, M. D. *et al.* (2011). *Acta Cryst.* D**67**, 235–242.